Semiclassical investigation of the revival phenomena in a one-dimensional system

2009 J. Phys. A: Math. Theor. 42 285304

(http://iopscience.iop.org/1751-8121/42/28/285304)

IOP PUBLISHING JOURNAL OF PHYSICS A: MATHEMATICAL AND THEORETICAL

J. Phys. A: Math. Theor. **42** (2009) 285304 (12pp) doi:10.1088/1751-8113/42/28/285304

Semiclassical investigation of the revival phenomena in a one-dimensional system

Zhe-xian Wang[1] **and Eric J Heller**[2]

[1] Hefei National Laboratory for Physical Sciences at Microscale and Department of Physics, University of Science and Technology of China, Hefei, Anhui 230026, People's Republic of China
[2] Department of Physics and Department of Chemistry and Chemical Biology, Harvard University, Cambridge, MA 02138, USA

Received 11 November 2008, in final form 3 June 2009
Published 24 June 2009
Online at stacks.iop.org/JPhysA/42/285304

Abstract

In a quantum revival, a localized wave packet re-forms or 'revives' into a compact reincarnation of itself long after it has spread in an unruly fashion over a region restricted only by the potential energy. This is a purely quantum phenomenon, which has no classical analog. Quantum revival and Anderson localization are members of a small class of subtle interference effects resulting in a quantum distribution radically different from the classical after long time evolution under classically nonlinear evolution. However, it is not clear that semiclassical methods, which start with the classical density and add interference effects, are in fact capable of capturing the revival phenomenon. Here we investigate two different one-dimensional systems, the infinite square well and Morse potential. In both the cases, after a long time the underlying classical manifolds are spread rather uniformly over phase space and are correspondingly spread in coordinate space, yet the semiclassical amplitudes are able to destructively interfere over most of coordinate space and constructively interfere in a small region, correctly reproducing a quantum revival. Further implications of this ability are discussed.

PACS numbers: 03.65.Sq, 42.50.Md

1. Introduction

The phenomenon of 'quantum revival' attracted much attention after it was first studied in quantum electrodynamics [1, 2]. The evolution of a quantum wave packet in a general smooth potential has at least three regimes. First, an initially localized packet will evolve following classical mechanics for a time, in the sense that the mean position and momentum of the wave packet follow classical laws. More than that, the spreading of the wave packet follows an analogous classical distribution with an appropriate initial position and momentum densities. This is the Ehrenfest regime.

After further evolution, after the wave packet becomes delocalized, interference effects may become important, causing the classical distribution and the quantum wave packet to have quite different details. Semiclassical methods, however, are expected to be working well [3–6]. They are based solely on classical information, but incorporate interference effects by assigning an amplitude and phase for the multiple classical paths which connect to each final position:

$$\psi(x,t) = \sum_n \sqrt{P_n(x,t)}\, \mathrm{e}^{\mathrm{i}\phi_n(x,t)/\hbar}, \tag{1}$$

where $P_n(x)$ is the classical probability density for the nth way of reaching x that gives the initial classical manifold and $\phi_n(x,t)$ is the classical action along the nth path of reaching x. The Born interpretation, namely that $\psi(x,t)$ is a probability amplitude, dictates that the wavefunction should go as the square root of the classical probabilities in the correspondence limit.

After a very long period of time, many classical periods in the case of an oscillator, the quantum wave packet will reverse its seemingly unorganized delocalized oscillation to neatly rebuild into its initial form. This is the known quantum revival, the third regime. Quantum revival has been widely investigated in atomic [7–10] and molecular [11–13] wave packet evolution and other quantum mechanics systems [14–18]. The work of Mallalieu *et al* [7] on the three-dimensional hydrogen atom is related to the present paper. An excellent review on wave packet revival is given by Robinett [19]. Precursors to the full revival also exist, in which other organized probability distributions develop [19]. The question addressed in this paper is: is the third revival regime also semiclassical? May we think of revival in semiclassical terms after all, i.e. classical mechanics with phase interference included? It is a large order for semiclassical sums to self-cancel almost everywhere where the classical density is large, with the exception of one region where the revival is occurring.

Time-dependent semiclassical methods are exact in the limit of short time, being equivalent to the short time limit of the quantum propagator. Increasing time can only degrade the results. Many times, the number of terms in the sum, equation (1), can become very large, and in fact the number of terms grows exponentially in chaotic systems. This in itself does not spell the breakdown of semiclassics. In earlier work on chaotic systems, Tomsovic *et al* [4] showed that semiclassical amplitudes were doing well when more than 6000 terms were needed in the sum. Other works justified the unexpected accuracy of the semiclassical results [5]. Later, Kaplan [6] gave an ingenious analysis of the breakdown with time in the case of chaotic systems, which built on the earlier analyses [5], indicating that the classical chaos rather surprisingly *aided* accurate semiclassical propagation. The implication was that even Anderson localization was describable semiclassically, albeit with an astronomical number of terms in the sum, equation (1). Quantum revival in a potential well does not involve chaotic spreading in phase space, and thus it would conceivably be more difficult to describe correctly semiclassically than chaotic dynamics, justifying the arguments in the above references about the benefits of chaotic flow.

The revival phenomenon has no purely classical analog. At best it is a semiclassical effect, described in terms of equation (1) [20]. The classical analog of a localized wave packet will be a continuous density of trajectories in phase space, well localized but consistent with the uncertainty principle. In an inharmonic oscillator, these trajectories occupy a distribution of energies and hence frequencies. The distribution spreads and begins to wind itself up on a spiral (see below), with many branches at a typical position. A smooth distribution of trajectories with a range of velocities and positions, after spreading evenly into the available space, will never converge again on one locale. This seems quite contradictory to the quantum

result. Semiclassical theory can bridge the gap between the classical and quantum field, and provide a simple and intuitive way to understand the subtle issue of quantum revival.

In this paper, we study the quantum revival in both an infinite square well and a Morse potential system. These two cases are quite different in detail. The square well is locally linear, interrupted by discontinuities which are due to reflections at the walls. The Morse potential is more typical, arriving at its nonlinear evolution smoothly. Semiclassical results are analytic whenever the dynamics is 'linear'. Examples are the free particle, the linear ramp potential and the harmonic oscillator. In each case, current positions and momenta are the linear functions of initial positions and momenta. The square well is not in fact a linear system because of reflections at the walls. However, locally, the classical manifolds evolve linearly, suffering truncation due to the reflections. Interestingly, the square well is a case with (globally) nonlinear time evolution clearly showing revivals, yet because of the locally linear nature of the classical dynamics the semiclassical formula turns out to be exact. When the semiclassical method is approximate, the delicate cancellation of amplitudes over wide areas is in question, and we show here by example that it is still accurate enough to give the revivals.

2. Theory

Time-dependent semiclassical methods face difficulties when applied to long revival time calculations. By their very nature, revivals cannot happen until the classical manifolds have folded over on themselves many times, which means that the dynamics is in the deeply nonlinear regime. Although nothing keeps semiclassical methods from working under these conditions in principle, and practice the error can only grow with time.If one is looking at a subtle phenomenon, such as near exact cancellation of semiclassical amplitudes over a wide area, the small errors could be a problem.

A convenient way to implement the semiclassical method is via cellular dynamics [23], which has been proven to be accurate and efficient for longtime implementation of semiclassical calculations. The basic idea is to linearize the classical dynamics in zones small enough to make the linearization classically correct. The zones are typically much smaller than Planck's constant in area. In the following, a brief summary of cellular dynamics is given. In the next section we discuss the revival in both infinite square well and Morse potential systems. Further speculations are given in the Conclusion section.

The starting point of the semiclassical method is the Van Vleck–Gutzwiller (VVG) propagator [24]:

$$\begin{aligned} G(x, x_0; t) &= \left(\frac{1}{2\pi \mathrm{i}\hbar}\right)^{1/2} \sum_j \left|\frac{\partial^2 S_j(x, x_0)}{\partial x \partial x_0}\right|^{1/2} \exp\left[\frac{\mathrm{i}S_j(x, x_0)}{\hbar} - \frac{\mathrm{i}\nu_j\pi}{2}\right] \\ &= \left(\frac{1}{2\pi \mathrm{i}\hbar}\right)^{1/2} \sum_j \left|\frac{\partial x}{\partial p_0}\right|^{-1/2} \exp\left[\frac{\mathrm{i}S_j(x, x_0)}{\hbar} - \frac{\mathrm{i}\nu_j\pi}{2}\right], \end{aligned} \tag{2}$$

where the action $S(x, x_0) = \int_0^t \mathrm{d}t'[p(t')\dot{x}(t') - H(p(t'), x(t'))]$ is the integral of the Lagrangian along classical trajectory from x_0 to x, and the Maslov index ν counts the number of caustic points along this trajectory. The sum over j runs over all the classical trajectories connecting x_0 to x; in other words, it counts in contributions from all the stationary phase points. Cellular dynamics begins with a transformation of the propagator by applying the speciality of the δ function:

$$\sum \frac{1}{(\partial x_t/\partial p_0)|_{x=x_t}} = \int \mathrm{d}p_0 \delta(x - x_t(x_0, p_0)). \tag{3}$$

Here, $x_t(x_0, p_0)$ is the final position originating from the initial point (x_0, p_0). The VVG propagator can now be written as

$$G(x, x_0; t) = \sqrt{\frac{1}{2\pi \mathrm{i}\hbar}} \int \mathrm{d}p_0 \left| \frac{\partial x_t}{\partial p_0} \right|_{x_0}^{1/2} \delta(x - x_t(x_0, p_0)) \exp\left[\frac{\mathrm{i}S(x_0, p_0)}{\hbar} - \frac{\mathrm{i}\upsilon\pi}{2} \right], \tag{4}$$

with the change of the action S as a function of (x_0, p_0). Then we can get the semiclassical wavefunction

$$\begin{aligned} \psi(x, t) &= \int \mathrm{d}x_0 G(x, x_0; t)\, \psi(x_0, 0) \\ &= \left(\frac{1}{2\pi \mathrm{i}\hbar} \right)^{1/2} \int \mathrm{d}x_0 \int \mathrm{d}p_0 \left| \frac{\partial x_t}{\partial p_0} \right|^{1/2} \delta(x - x_t)\, \mathrm{e}^{\mathrm{i}S/\hbar - \mathrm{i}\upsilon\pi/2} \psi(x_0, 0). \end{aligned} \tag{5}$$

It would be difficult to evaluate the integral directly since it is highly oscillatory. However, cellular dynamics handles this difficulty by using integration techniques similar in spirit to Filinov methods [25], by dividing the region into small cells, inserting the identities $1 \approx \eta \sum_n \exp[-\alpha(x - x_n)^2]$ within both x and p spaces. Then we have

$$\begin{aligned} \psi(x, t) \approx \eta\eta' \sum_n \sum_m \int \mathrm{d}x_0 \int \mathrm{d}p_0 \left| \frac{\partial x_t}{\partial p_0} \right|^{1/2} \delta(x - x_t)\, \mathrm{e}^{\mathrm{i}S/\hbar - \mathrm{i}\upsilon\pi/2} \\ \times \mathrm{e}^{-\alpha(x_0 - x_n)^2 - \beta(p_0 - p_m)^2}\, \mathrm{e}^{-\gamma(x_0 - x_i)^2 + \mathrm{i}k_i(x_0 - x_i)^2}, \end{aligned} \tag{6}$$

where the initial wavefunction $\psi(x_0, 0) = \exp[-\gamma(x_0 - x_i)^2 + \mathrm{i}k_i(x_0 - x_i)^2]$ is used. If both α and β are taken to be sufficiently large, and for sufficiently many cells, this expression becomes identical to the usual primitive semiclassical propagator. Thus, even though it resembles an initial value representation, it is not. We can linearize the classical dynamics around the central trajectory for each cell running from the initial phase space point (x_n, p_m), obtaining its contribution to the propagation of initial wavefunction.

In some ways cellular dynamics resembles Miller's initial value representation (IVR) [26], but there are important differences. The IVR is actually numerically superior, in that if the integral is performed the result is not the 'primitive semiclassical' Van Vleck result, but rather a uniformized version which is capable of describing some classically forbidden processes and of smoothing out some semiclassical singularities. In contrast, cellular dynamics is a direct but numerically convenient implementation of the primitive semiclassical Green's function. For further reading, a rather general summary of the relationship between different expressions of propagator is given by Kay [27], where another frequently used Heller–Herman–Kluk–Kay IVR [28] is also included. The goal of the present paper is to test the efficacy of the primitive semiclassical propagator, but implementing an IVR would be an interesting study.

The linearization is implemented by approximating the classical action S with the second-order Taylor expansion and the final position x (x_0, p_0) with first order [23], namely

$$\begin{aligned} S &\approx S_{nmt} + (p_{nmt} m_{22} - p_m)(x_0 - x_n) + p_{nmt} m_{21}(p_0 - p_m) + \tfrac{1}{2} m_{12} m_{22}(x_0 - x_n)^2 \\ &\quad + \tfrac{1}{2} m_{11} m_{21}(p_0 - p_m)^2 + m_{12} m_{21}(x_0 - x_n)(p_0 - p_m) \\ x_t(x_0, p_0) &\approx x_{nmt} + m_{21}(p_0 - p_m) + m_{22}(x_0 - x_n), \end{aligned} \tag{7}$$

where $S_{nmt}, x_{nmt}, p_{nmt}$ are the classical action, final position and momentum of a trajectory originating from (x_n, p_m) respectively, and

$$M = \begin{pmatrix} m_{11} & m_{12} \\ m_{21} & m_{22} \end{pmatrix} = \begin{pmatrix} \partial p_t/\partial p_0 & \partial p_t/\partial x_0 \\ \partial x_t/\partial p_0 & \partial x_t/\partial x_0 \end{pmatrix} \tag{8}$$

is the Jacobian matrix of the corresponding dynamical transformation [23]. The substitution of equation (7) into (6) will simplify the quadrature into Gaussian integration

$$\psi(x,t) \approx \eta\eta' \sum_n \sum_m \int \mathrm{d}x_0 \left|\frac{\partial x_t}{\partial p_0}\right|^{-1/2} \mathrm{e}^{-a(x_0-x_n)^2+b(x_0-x_n)+c}, \tag{9}$$

with the coefficients

$$\begin{aligned}
a &= \alpha+\gamma+\beta\left(\frac{m_{22}}{m_{21}}\right)^2 - \frac{\mathrm{i}}{\hbar}\left(\frac{1}{2}\frac{m_{11}m_{22}^2}{m_{21}} - \frac{1}{2}m_{12}m_{22}\right),\\
b &= \frac{2\beta m_{22}}{m_{21}^2}(x-x_{nmt}) - 2\gamma(x_n-x_i) + \mathrm{i}k_i + \frac{\mathrm{i}}{\hbar}\left[\left(m_{12}-\frac{m_{11}m_{22}}{m_{21}}\right)(x-x_{nmt}) - p_m\right],\\
c &= -\frac{\beta}{m_{21}^2}(x-x_{nmt})^2 - \gamma(x_n-x_i)^2 - \frac{\mathrm{i}\nu\pi}{2} + \mathrm{i}k_i(x_n-x_i)\\
&\quad + \frac{\mathrm{i}}{\hbar}\left[S_{nmt} + p_{nmt}(x-x_{nmt}) + \frac{m_{11}}{2m_{21}}(x-x_{nmt})^2\right].
\end{aligned} \tag{10}$$

Equation (6) can now be analytically evaluated:

$$\psi(x,t) \approx \eta\eta' \sum_n \sum_m \sqrt{\frac{\pi}{am_{21}}}\, \mathrm{e}^{b^2/4a+c}, \tag{11}$$

and it is easy to implement.

3. Results and discussions

In this section, we will analyze the quantum revival in the infinite square well and the Morse potential in detail. First we look at the infinite square well system, which has been well studied at many levels and from many points of view [16–18]. The system Hamiltonian is

$$H = p^2/2m + V(x), \qquad V(x) = \begin{cases} 0, & 0 < x < L \\ \infty, & x \leqslant 0, \quad x \geqslant L, \end{cases} \tag{12}$$

and by using the eigenstate expansion

$$\psi(x_0,t) = \sum_{n=1}^{\infty} C_n \varphi_n(x_0)\, \mathrm{e}^{-\mathrm{i}E_n t/\hbar}, \qquad C_n = \int_0^L \psi(x_0,t)\varphi_n^*(x_0)\,\mathrm{d}x_0 \tag{13}$$

($E_n, \varphi_n(x_0)$ are the eigenvalue and eigenfunction of the infinite square well, respectively) we show the schematic evolution of an initial Gaussian wave packet $\psi(x_0,0) = \sqrt{\gamma/\pi}\exp[-\gamma(x_0-x_i)^2 + \mathrm{i}k_i(x_0-x_i)]$ in the well in figure 1(*a*). Here the parameters $\gamma = 0.02, k_i = 2, x_i = 50, L = 80$ are taken, and $m = 1, \hbar = 1$ are used throughout the paper for simplicity. And for the infinite square well system, the revival time can be analytically determined as $T_{\mathrm{rev}} = 4mL^2/\hbar\pi$ [17]. As we see from figure 1(*a*), the wave packet delocalizes and spreads all over the well after first several classical periods. At half the revival time, $t = T_{\mathrm{rev}}/2$, the wavefunction is nearly a mirror image of the initial wavefunction. At the revival time T_{rev} the wavefunction is perfectly rebuilt into the initial wave packet. In the following we do it in a semiclassical way to describe this surprising relocalization of the wave packet.

There is an analytical semiclassical solution for the infinite square well, even though it is a globally nonlinear system. The semiclassical propagator $G(x, x_0; t)$ can be written as a summation of contributions from all the stationary phase points which correspond to classical trajectories connecting x_0 and x_t [30, 31]. As shown in figure 1(*b*), these trajectories can

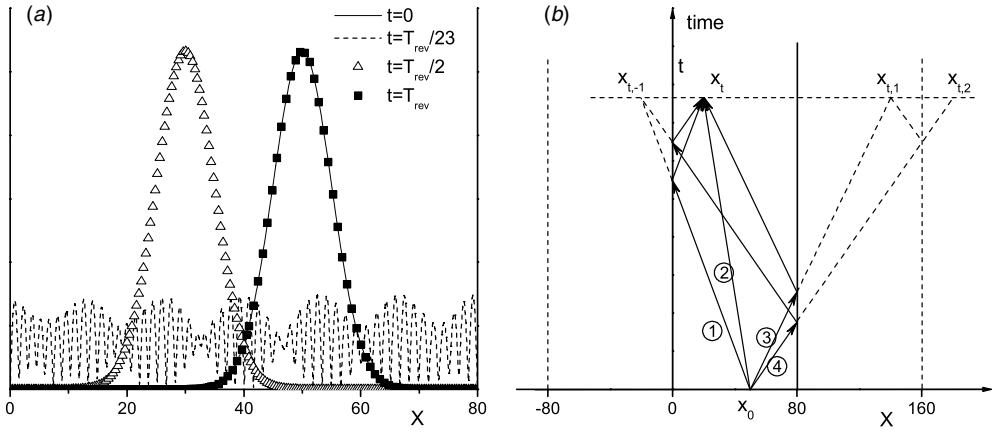

Figure 1. (*a*) Gaussian wave packet evolves in an infinite square well at different times. (*b*) Classical trajectories starting from x_0 and end at x_t at time t. $x_{t,-1}, x_{t,1}, x_{t,2}$ are image points of x_t, the trajectories ①, ③ bounce off the wall an odd number of times and ②, ④ an even number of times.

be divided into two groups; they are reflected by the wall an odd and even number of times respectively. So we have

$$\begin{aligned} G(x, x_0; t) &= \sqrt{\frac{m}{2\pi \mathrm{i}\hbar t}} \left[\sum_{n=-\infty}^{\infty} \exp\left(\frac{\mathrm{i}m(-x - x_0 + 2nL)^2}{2\hbar t} - \mathrm{i}|2n-1|\pi \right) \right. \\ &\quad \left. + \sum_{n=-\infty}^{\infty} \exp\left(\frac{\mathrm{i}m(x - x_0 + 2nL)^2}{2\hbar t} - \mathrm{i}|2n|\pi \right) \right] \\ &= \sqrt{\frac{m}{2\pi \mathrm{i}\hbar t}} \left[\sum_{n=-\infty}^{\infty} \exp\left(\frac{\mathrm{i}m(x - x_0 + 2nL)^2}{2\hbar t} \right) \right. \\ &\quad \left. - \sum_{n=-\infty}^{\infty} \exp\left(\frac{\mathrm{i}m(-x - x_0 + 2nL)^2}{2\hbar t} \right) \right]. \end{aligned} \tag{14}$$

The exponents of two exponential functions here are composed of the classical action and Maslov phase, and one should note that in the hard wall limit the Maslov phase is a multiple of π instead of $\pi/2$. Then using the Jacobi theta function $\vartheta_3(z, T) = \sum_{n=-\infty}^{\infty} \exp[\mathrm{i}\pi(n^2 T + 2nz)]$ and its important property [32]

$$\vartheta_3(z, T) = \sqrt{\mathrm{i}/T}\, \exp(z^2/\mathrm{i}\pi T)\vartheta_3(z/T, -1/T), \tag{15}$$

we simplify equation (14) into

$$\begin{aligned} G(x, x_0; t) &= \frac{1}{2L}\left[\vartheta_3\left(\frac{x - x_0}{2L}, \frac{-\pi\hbar t}{2mL^2} \right) - \vartheta_3\left(\frac{x + x_0}{2L}, \frac{-\pi\hbar t}{2mL^2} \right) \right] \\ &= \frac{1}{2L} \sum_{n=-\infty}^{\infty} \exp\left(\frac{-\mathrm{i}n^2\pi^2\hbar t}{2mL^2} \right) \left[\exp\left(\frac{\mathrm{i}n\pi(x - x_0)}{L} \right) - \exp\left(\frac{-\mathrm{i}n\pi(x + x_0)}{L} \right) \right] \\ &= \frac{2}{L} \sum_{n=1}^{\infty} \exp\left(\frac{-\mathrm{i}n^2\pi^2\hbar t}{2mL^2} \right) \sin\left(\frac{n\pi x_0}{L} \right) \sin\left(\frac{n\pi x}{L} \right). \end{aligned} \tag{16}$$

This is identical to the usual quantum propagator in the infinite square well. The semiclassical propagator at the revival time $t = T_{\text{rev}} = 4mL^2/\hbar\pi$ can thus be written as

$$G(x, x_0; T_{\text{rev}}) = \frac{1}{2L}\sum_{n=-\infty}^{\infty} \exp\left[\frac{\mathrm{i}n\pi(x - x_0)}{L}\right] - \frac{1}{2L}\sum_{n=-\infty}^{\infty} \exp\left[\frac{-\mathrm{i}n\pi(x + x_0)}{L}\right]$$
$$= \delta(x - x_0) - \delta(x + x_0), \tag{17}$$

where the discrete Fourier transform of the δ function is used. Then we have the semiclassical wavefunction in the square well region $0 < x < L$:

$$\begin{aligned}\psi(x, T_{\text{rev}}) &= \int_0^L \mathrm{d}x_0 G(x, x_0; T_{\text{rev}})\psi(x_0, 0)\\ &= \int_0^L \mathrm{d}x_0[\delta(x - x_0) - \delta(x + x_0)]\psi(x_0, 0)\\ &= \int_0^L \mathrm{d}x_0\delta(x - x_0)\psi(x_0, 0)\\ &= \psi(x, 0),\end{aligned} \tag{18}$$

namely the revival occurs. Equations (14), (17) and (18) explicitly show that the revival of the wave packet is essentially an effect of interference between classical trajectories, only those trajectories bouncing off the boundary an even number times contribute to the revival, whereas others interfere destructively and hence give no contribution.

Now we come to see a more general system, the Morse potential; it is also a widely used model in many fields. There is no exact solution for wave packet evolution in the Morse potential; we give the precise numerical results below using FFT and semiclassical results by using cellular dynamics. We take $V(x) = D[1 - \exp(-\lambda x)]^2$ with $D = 150, \lambda = 0.288$; its revival time $T_{\text{rev}} = 2m\pi/(\hbar\lambda)^2$ can be derived by expanding the wavefunction with eigenfunctions of the Morse potential, too (see appendix A). Approximating the Morse potential $V(x)$ with the Taylor series to second order $V(x) \approx D\lambda^2x^2 = m\omega^2x^2/2$ leads to a coarse classical period $T_{cl} = 2\pi/\omega = 2\pi/\sqrt{2D\lambda^2/m}$, and then the revival time here is about 60 times of the classical period. With $\alpha = 5000, \beta = 312.5$ being used in the calculation, the semiclassical wavefunctions originate from $\psi(x_0, 0) = \sqrt{\gamma/\pi}\exp[-\gamma(x_0 - x_i)^2](\gamma = 2, x_i = 3.5)$ are depicted in figure 2.

Comparing to the FFT exact wavefunctions we can see that semiclassical wavefunctions agree well for different timescales, showing the capability of semiclassical approximation in long-time nonlinear dynamics. In figure 2, we also plot the normalized purely classical density derived by removing the phase terms $\mathrm{e}^{\mathrm{i}S/\hbar - \mathrm{i}\nu\pi/2}$ in equation (5), since the semiclassical result consists of different classical trajectories with the square root of classical probabilities and phase information, omitting the interference effect between the trajectories namely removing phase terms will lead to a purely classical result. It is remarkable that despite the fact that the classical densities are spread all over the available space, the semiclassical approximation can still build a localized wave packet.

In order to demonstrate how the information carried by classical trajectories yields a revival of the wave packet, we first Wigner transform the initial Gaussian distribution $\psi(x) = \sqrt{\gamma/\pi}\exp[-\gamma(x - x_i)^2]$,

$$\begin{aligned}W(x, p) &= \frac{1}{\pi\hbar}\int_{-\infty}^{\infty} \psi^*(x - s)\psi(x + s)\,\mathrm{e}^{\mathrm{i}2ps/\hbar}\,\mathrm{d}s\\ &= \frac{\gamma}{\pi^2\hbar}\int_{-\infty}^{\infty} \mathrm{e}^{-\gamma(x - x_i - s)^2}\,\mathrm{e}^{-\gamma(x - x_i + s)^2}\,\mathrm{e}^{\mathrm{i}2ps/\hbar}\,\mathrm{d}s\end{aligned}$$

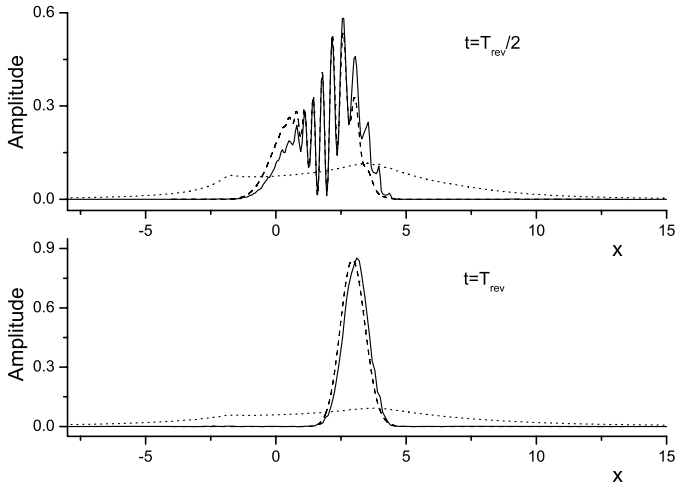

Figure 2. Wavefunctions and classical distribution probabilities in the Morse potential at times $T_{\rm rev}/2$ and $T_{\rm rev}$. All the functions plotted in this figure are normalized. Solid line: semiclassical wavefunctions; dashed line: exact FFT wavefunctions calculated by the split–operator method [29]; dotted line: classical distribution probability.

$$= \frac{\gamma}{\pi^2\hbar}\int_{-\infty}^{\infty} \mathrm{e}^{-2\gamma(x-x_i)^2-2\gamma s^2+\mathrm{i}2ps/\hbar}\,\mathrm{d}s$$
$$= \sqrt{\frac{\gamma}{2\pi^3\hbar^2}}\,\mathrm{e}^{-p^2/2\gamma\hbar-2\gamma(x-x_i)^2}, \tag{19}$$

which is itself a Gaussian, and then watch the evolution of this Wigner distribution in phase space. The corresponding starting swarm of classical trajectories emerges as an elliptical disk in phase space; as time evolves this ellipse stretches and twists, forming a large whorl. (Indeed, the time evolution of the phase space is that of an area preserving twist map.) In figure 3, we plot its final phase space distribution at the revival time $t = T_{\rm rev}$; the color of each point indicates phase information carried by corresponding classical trajectory.

The coordinate space density is the projection of the phase space density onto coordinate space, including the addition of phase which here is given by color. The phase changes along the whorl too. It changes rapidly over the shallow region of potential but varies slowly at both the ends. The buildup in coordinate space can only occur where there are trajectories in phase space which are of the same or similar color lined up above and below the given region of coordinate. In appendix B, we prove that the classical action difference between the two points equals the enclosed area of the manifold. This explains why there are similar classical actions near the turning point regimes at both the ends (see figure 3(*a*)) due to the small enclosed areas. The abrupt change of colors at the turning points is due to the change in the Maslov phase.

According to equation (1), the semiclassical wavefunction $\psi(x, T_{\rm rev})$ comes from the contributions of stationary phase points which are produced by the intersection of the manifold with the position state $|x\rangle$, and it will give out big amplitude if these stationary phase points have large magnitude $P_n(x, t)$ and similar phases. The blurred phase space diagram in figure 3(*b*) clearly shows the monochromatic bright colored regions indicating adjacent classical manifolds with similar phases, whereas other parts are averaged out and give neutral

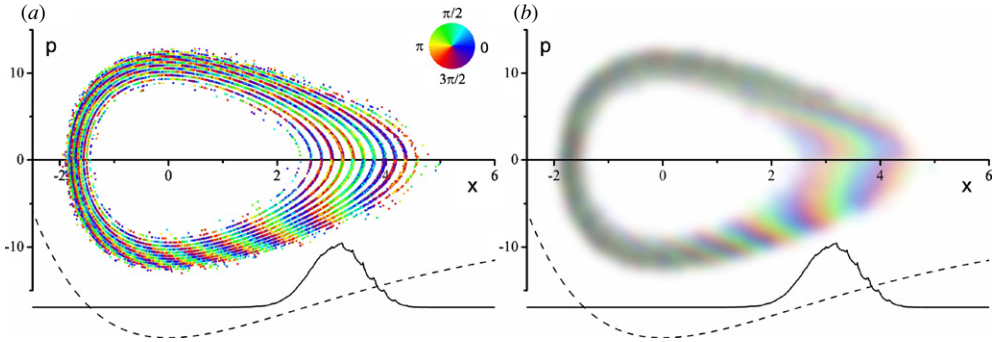

Figure 3. (*a*) The transient phase space diagram for the time evolved initial Gaussian (the Wigner transform of the initial state) evolves in the Morse potential to the revival time $T_{\rm rev}$. The color represents different values of the semiclassical phase (including the classical action S and the Maslov phase) modulo $[0, 2\pi]$. (*b*) The Gaussian blurred version of (*a*). Solid line: semiclassical wavefunction at time $T_{\rm rev}$; dashed line: Morse potential.

(This figure is in colour only in the electronic version)

gray colors. Combined with the large magnitude $P_n(x, t)$ they carry, the regions of saturated color correctly produce the wave packet revival.

One could still doubt why we do not get a high amplitude wavefunction at the left end of the whorl, where a caustic pileup of manifold at a similar position occurs corresponding to the classical probability density which goes as the inverse of the momentum. Moreover, as we have just said, the phase is not changing there, except for the abrupt Maslov phase. To compare the difference, we write the formula of the wavefunction into a compact form:

$$\begin{aligned}\psi(x, T_{\rm rev}) &= \int {\rm d}x_0 G(x, x_0; T_{\rm rev})\psi(x_0, 0) \\ &= \sqrt{\frac{1}{2\pi {\rm i}\hbar}} \int {\rm d}x_0 \sum_j \left|\frac{\partial x}{\partial p_0}\right|^{-1/2} \exp\left[\frac{{\rm i}S_j(x, x_i)}{\hbar} - {\rm i}\upsilon_j\pi\right]\psi(x_0, 0) \\ &= \int {\rm d}x_0 R\, {\rm e}^{{\rm i}\phi} = \sum_n R_n\, {\rm e}^{{\rm i}\phi_n}\Delta x_0. \end{aligned} \tag{20}$$

The integral can be done numerically by a finite sum of a complex vector. We divide x space into hundreds of sections, and evaluate the vector separately in each section. By drawing each vector from the tips of the previous one, the summation form a chain, and the line drawn from first point to the end point represent the quadrature. We draw two chains respectively for $x = -1.6$ and $x = 3.1$ in figure 4.

For the low amplitude region $x = -1.6$, the chain circles continuously, and results in a small total vector (see figure 4(*a*)). This indicates that the phase of stationary phase points changes rapidly and continuously, leading to destructive interference betweenclassical trajectories and a small amplitude of the wavefunction. A different situation appears in figure 4(*b*) for the position $x = 3.1$. Here the small phase difference between stationary points accumulates a persistent growth of the total vector; namely the constructive interference produces high amplitude of wavefunction. The probability density is about 25 times larger for region (b) than (a).

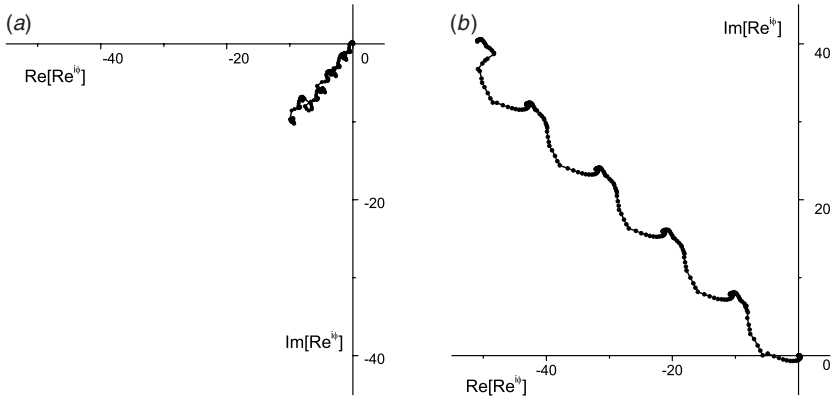

Figure 4. (*a*) Vector chain for $x = -1.6$. (*b*) Vector chain for $x = 3.1$.

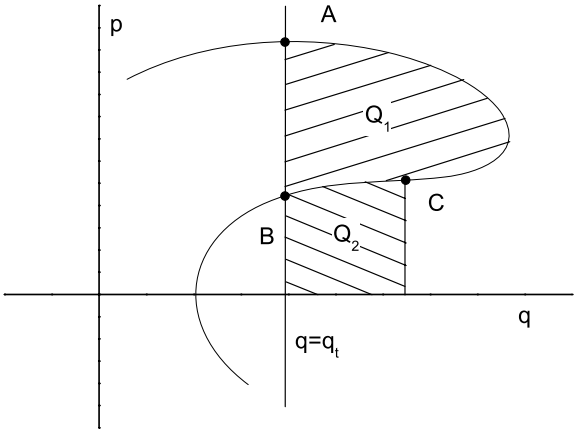

Figure 5. Classical manifold. The area contained between intersections of the manifold $p(q)$ and a position state (vertical line $q = q_t$) is Q_1.

4. Conclusions and discussion

Whenever and wherever they apply, semiclassical methods can be extremely useful not only in computations but also in providing an underlying intuition for quantum phenomena. Here we have shown that something so subtle as a quantum revival still has classical underpinnings, as seen by the successful construction of the phenomenon using only classical mechanics as input. Semiclassical methods are accurate enough to describe the quantum revival phenomenon. The quantum revival phenomenon does not stem from an accumulation of classical trajectories. Rather, the classical trajectories are rather uniformly spread, and it is through destructive interference of the semiclassical amplitudes that the wavefunction is canceled in most places.

Acknowledgments

One of us (ZXW) would like to acknowledge helpful discussions with Brian Landry. This work was supported in part by the National Natural Science Foundation of China (grant nos

10574121 and 10874160), '111' Project, Chinese Education Ministry and Chinese Academy of Sciences.

Appendix A

For the Morse potential $V(x) = D[1 - \exp(-\lambda x)]^2$, one can express the time-dependent wavefunction in terms of eigenfunctions $\varphi_n(x)$, via

$$\psi(x,t) = \sum_{n=0}^{\infty} a_n \varphi_n(x)\, \mathrm{e}^{-\mathrm{i}E_n t/\hbar}, \tag{A.1}$$

where the eigenvalues are $E_n = \alpha(n+1/2) - \beta(n+1/2)^2$ with $\alpha = \hbar\lambda\sqrt{2D/m}$, $\beta = \hbar^2\lambda^2/2m$. The revival condition $\psi(x,T) = \psi(x,0)$ requires

$$E_n T = [\alpha(n+1/2) - \beta(n+1/2)^2]T = 2M_n\pi, \tag{A.2}$$

where M_n are integers. Make a subtraction of consecutive n of equation (A.2) gives

$$(\alpha - 2\beta n - 2\beta)T = 2K_n\pi, \tag{A.3}$$

with K_n are also integers. Then apply the subtraction (A.3) again, and obtain the equation for the shortest revival time T_{rev} as

$$2\beta T_{\mathrm{rev}} = 2\pi. \tag{A.4}$$

So we have the revival time $T_{\mathrm{rev}} = \pi/\beta = 2m\pi/(\hbar\lambda)^2$.

Appendix B

We prove the standard result that the difference of the classical actions S_A and S_B equals to the shaded area Q_1. First we look at points B and C. From the classical action formula $S = \int p(q)\,\mathrm{d}q + \int H(p,q)\,\mathrm{d}t$ we have $\partial S/\partial q = p$; thus the action difference from B to C is

$$S_C - S_B = \int_B^C \frac{\partial S}{\partial q}\,\mathrm{d}q = \int_B^C p\,\mathrm{d}q = \text{area} \quad Q_2. \tag{B.1}$$

Then, in a similar way

$$S_A - S_B = \int_B^A \frac{\partial S}{\partial q}\,\mathrm{d}q = \int_B^A p\,\mathrm{d}q = \text{area} \quad Q_1. \tag{B.2}$$

References

[1] Eberly J H, Narozhny N B and Sanchez-Mondragon J J 1980 *Phys. Rev. Lett.* **44** 1323
[2] Narozhny N B, Sanchez-Mondragon J J and Eberly J H 1981 *Phys. Rev.* A **23** 236
[3] O'Connor P W, Tomsovic S and Heller E J 1992 *J. Stat. Phys.* **68** 131
[4] Tomsovic S and Heller E J 1991 *Phys. Rev. Lett.* **67** 664
[5] Tomsovic S and Heller E J 1993 *Phys. Rev.* E **47** 282
[6] Kaplan L 1998 *Phys. Rev. Lett.* **81** 3371
Kaplan L and Heller E J 1996 *Phys. Rev. Lett.* **76** 1453
[7] Mallalieu M and Stroud C R Jr 1994 *Phys. Rev.* A **49** 2329
[8] Parker J and Stroud C R Jr 1986 *Phys. Rev. Lett.* **56** 716
[9] Parker J and Stroud C R Jr 1986 *Phys. Scr.* T **12** 70
[10] Alber G and Zoller P 1991 *Phys. Rep.* **199** 231
[11] Fischer I, Villeneuve D M, Vrakking M J J and Stolow A 1995 *J. Chem. Phys.* **102** 5566
[12] Vrakking M J J, Villeneuve D M and Stolow A 1996 *Phys. Rev.* A **54** R37

[13] Doncheski M A and Robinett R W 2003 *Ann. Phys.* **308** 578
[14] Aronstein D L and Stroud C R Jr 2000 *Phys. Rev.* A **62** 022102
[15] Vetchinkin S I and Eryomin V V 1994 *Chem. Phys. Lett.* **222** 394
[16] Robinett R W 2000 *Am. J. Phys.* **68** 410
[17] Styer D F 2001 *Am. J. Phys.* **69** 56
[18] Waldenstrom S, Naqvi K R and Mork K J 2003 *Phys. Scr.* **68** 45
[19] Robinett R W 2004 *Phys. Rep.* **392** 1
[20] Brouwer P W and Altland A 2008 *Phys. Rev.* B **78** 075304
[21] Heller E J 1975 *J. Chem. Phys.* **62** 1544
[22] Littlejhon R G 1986 *Phys. Rep.* **138** 193
[23] Heller E J 1991 *J. Chem. Phys.* **94** 2723
[24] Gutzwiller M C 1967 *J. Math. Phys.* **8** 1979
[25] Filinov V S 1986 *Nucl. Phys.* B **271** 717
[26] Miller W H 2001 *J. Phys. Chem.* A **105** 2942
[27] Kay K G 1994 *J. Chem. Phys.* **100** 4377
[28] Herman M F and Kluk E 1984 *Chem. Phys.* **91** 27
[29] Feit M D, Fleck J A Jr and Steiger A 1982 *J. Comput. Phys.* **47** 412
[30] Goodman M 1981 *Am. J. Phys.* **49** 843
[31] Grosche C and Steiner F 1998 *Handbook of Feynman Path Integrals* (New York: Springer)
[32] Abramowitz M and Stegun I A 1964 *Handbook of Mathematical Functions with Formulas, Graphs, and Mathematical Tables* (Washington: U.S. Government Print Office)
[33] Topinka M A, LeRoy B J, Westervelt R M, Shaw S E J, Fleischmann R, Heller E J, Maranowski K D and Gossard A C 2001 *Nature* **410** 183
[34] Heller E J and Shaw S 2003 *Int. J. Mod. Phys.* B **17** 3977